Current Research in Food Science 5 (2022) 743–751

Contents lists available at ScienceDirect

Current Research in Food Science

journal homepage: www.sciencedirect.com/journal/current-research-in-food-science

pH indicator films fabricated from soy protein isolate modified with chitin nanowhisker and *Clitoria ternatea* flower extract

Rekha Rose Koshy [a,b], Arunima Reghunadhan [c], Siji K. Mary [a,b], Prasanth S. Pillai [d], Seno Joseph [b], Laly A. Pothen [b,e,*]

[a] Postgraduate and Research Department of Chemistry, Bishop Moore College, Mavelikara, 690101, Kerala, India
[b] Postgraduate and Research Department of Chemistry, CMS College, Kottayam, 686001, Kerala, India
[c] Department of Chemistry, TKM College of Engineering, Karicode, Kollam, Kerala, 691005, India
[d] University of Saskatchewan, Saskatoon, SK, Canada
[e] International and Interuniversity Centre for Nanoscience and Nanotechnology, Mahatma Gandhi University Kottayam, India

ARTICLE INFO

Keywords:
pH sensitive film
Soy protein isolate
Steam explosion
Chitin nanowhisker
CO_2 detection

ABSTRACT

Sensor films are finding wide range of applications. Different type of sensing films is fabricated for the identification of chemicals, ions, heavy metals, changes in the pH, etc. The present report is on the fabrication of pH sensitive films from completely natural sources-soy protein isolate, chitin nano whiskers and flower extract. The highly crystalline chitin nano whiskers (CNW) were extracted from prawn shell under neutral condition via steam explosion technique. Multifunctional Soy protein isolate (SPI) films were prepared by adding chitin nanowhisker and *Clitoria ternatea* flower extract and its effect on thermal, mechanical and moisture properties of SPI film was investigated. The isolated CNW presented a needle like morphology with a diameter of 10–50 nm and a crystallinity index of 99.67%. The extracted chitin nanowhisker was used to prepare biodegradable films with soy protein isolate immobilized with anthocyanin from *Clitoria ternatea* flower extract. The prepared Soy protein -chitin nanowhisker films was found to have a tensile strength of about 15.45 ± 0.97 MPa with 8% chitin nanowhisker addition. The addition of CTE was found to decrease the tensile strength of SPI-CNW film but was found to make the film pH sensitive. The developed indicator film showed visible color changes in acidic and basic medium and hence can be used to monitor the freshness of food materials.

1. Introduction

Active and intelligent packaging is a novel development in the area of packaging wherein a packaging material benefits from synergistic effect of both active (antimicrobial and antioxidant) and intelligent part (indicating about the product freshness, temperature, safety etc.) (Silva-Pereira et al., 2015; Ahmad et al., 2019) Biodegradable polymers are a strong choice among researchers for making these types of materials since it will reduce the dependence on petroleum derived plastics and reduce environmental pollution. Renewable and readily useable biopolymers such as proteins, polysaccharides, enzymes, lipids and their mixtures are the most viable substitutes for the manufacture of renewable materials in the near future. Among these biopolymers, soy protein, is a good alternative to petroleum-based products since it is biocompatible, renewable, biodegradable, and has good film-forming abilities (Zolfi et al., 2014). Soy protein is a protein derived from soybean and is obtained as a byproduct of soy oil production. Compared to other biopolymers, soy protein has excellent barrier and film-forming properties due to the presence of 18 different amino acids which provide abundant polar groups for bond formation, which may in turn improve the mechanical and physical properties of the protein during film formation. However, the inherent hydrophilic and brittle nature of soy protein isolate limits the practical value of the matrix.

Nanomaterials is always found to enhance the properties of soy protein films due to its size, distribution and morphology. Chitin nanowhisker (CNW) is one such nanoparticle, which is widely used to reinforce soy protein composites. CNW is isolated from chitin which is present in arthropod exoskeleton like that of insects and crustaceans viz. crabs, lobsters and shrimps, the cell wall of molluscs and fungi, beaks and internal shells of cephalopods like octopuses and squids. Chitin is a derivative of glucose which contains the monomer N-acetylglucosamine arranged in a linear fashion and is natural, non-allergic, non-toxic,

* Corresponding author. Postgraduate and Research Department of Chemistry, CMS College, Kottayam, 686001, Kerala, India.
E-mail address: lapothen@gmail.com (L.A. Pothen).

https://doi.org/10.1016/j.crfs.2022.03.015
Received 16 November 2021; Received in revised form 12 March 2022; Accepted 25 March 2022
Available online 14 April 2022

biodegradable, anti-microbial, water insoluble and resistant to many organic solvents. Because of their distinct physical and chemical properties along with their antibacterial activity, chitin nano whiskers serve as the most cost-efficient alternative in pharmaceuticals, cosmetics and packaging of food. Several methods employed for the preparation of CNW, nanocrystals or nanofibers are mechanical treatment, electrospinning (Ifuku and Saimoto, 2012), acid hydrolysis (Ifuku et al., 2010), ultrasonication (Lu et al., 2013) and TEMPO-mediated oxidation (Ifuku and Saimoto, 2012). However, these methods for extraction of CNW are time consuming, tedious and require several treatments and washing steps. Along with that, acetic acid is added to prevent the aggregation of CNW, which may in turn pose problems during application of CNW in biomedical materials, electronics devices, nanocomposites, and so on (Ifuku et al., 2011). Hence there is the need for the development of effective and simple processing methods to isolate CNW economically and without severe degradation.

In the present study, steam explosion technique is used for the extraction of CNW from the prawn shells wherein, an autoclave is used. It is providing an economic way to extract highly crystalline CNW within one day. This method involves the application of extremely high pressure on prawn shell waste to divide large particles into very small sizes of the order of nanometer magnitude. Many researchers have been studying the treatment of various biomass resources by steam explosion but all these works deal with the preparation of nano objects for cellulose (Kaushik et al., 2010; Deepa et al., 2011; Vijayalakshmi et al., 2016). This is believed to be the first report on the preparation of CNW by steam explosion technique employing economically viable autoclave. Using this pressure-assisted technique, individualized α-chitin nano-whiskers with a diameter of less than 100 nm have been processed and this methodology provides a versatile, scalable, viable and environmentally friendly way to process CNW on a large scale. Also, in this method acetic acid is not used and hence CNW under neutral condition is obtained.

Anthocyanin the phenolic pigment responsible for color in fruits, vegetables and flowers has the ability to present different chemical structures in different pH (Yun et al., 2019). Therefore, anthocyanin-rich films are regarded as promising intelligent pH indicators as the structural changes of anthocyanin in different pH is accompanied by corresponding color changes which can be visually monitored. Hence anthocyanin is commonly used to monitor food freshness as food spoilage is usually accompanied by pH changes. Anthocyanins also possess antioxidant and antibacterial properties and hence when incorporated in packaging films can delay the deterioration process of the packed material. Till now anthocyanins extracted from several fruits, flower and vegetable sources like blueberry (Luchese et al., 2018), bayberry (Yun et al., 2019) red cabbage (Silva-Pereira et al., 2015),etc. have been added into polymer matrices to impart pH sensing ability to films. ClitoriaTernatea/Butterfly pea flower extract is also an excellent source of anthocyanin but little literature data is available on the use of this flower extract in polymer matrix.

Clitoria ternatea (CT) also known as “Butterfly Pea”, “Bunga Telang” or “Blue Pea” belongs to Leguminosae family and contains (poly) acylated anthocyanins, ternatins in its petals. The flower is bright blue in color and this blue color is attributed to the anthocyanin, delphinidin glycoside (Ahmad et al., 2019). The anthocyanin from Clitoria ternatea can be used to monitor freshness of packed food (Choi et al., 2017)since during the deterioration process happening in food, acids and other volatile components are released, pH changes occur and anthocyanin changes color according to pH changes.

Herein, we report the preparation of novel pH indicator film made from soy protein isolate reinforced with chitin nanowhisker and anthocyanin rich Clitoria ternatea extract (CTE). Very few reports are available on SPI-CNW composites and the existing literature reports a highest tensile strength 8.4 MPa with 20% CNW but in this study, we could achieve a tensile strength of 15 MPa with 8%CNW addition.

2. Material and methods

2.1. Materials and reagent

SPI with protein content of 95% was purchased from Adeesh Agrofood, Haryana. Clitoria ternatea flower was plucked from neighbourhood. Chitin (viscosity [0.5%-AA & CS at 20 °C]: 800–940 cps, ash <5%, particle size: 3 mm) obtained from prawn shell was procured from Marine Chemicals, Kochi and used without any modification.

2.2. Isolation of chitin nano whisker (CNW)

To isolate CNW from raw chitin, the prawn shells waste was subjected mainly 3 process: deproteinization, demineralization and decolorization. In the deproteinization step, about 40 g of wet prawn shells waste were treated with 3N NaOH under pressure in an autoclave at a pressure of 10 lb and at a temperature of 110–120 °C for half an hour to remove most of the protein. After releasing the ppressure immediately, chitin was taken from the autoclave and washed with water until the pH was neutral. In the demineralization step, the suspension was then treated with 2N HCl in the autoclave for half an hour until it attained a pressure of 10 lb (517.14 mm Hg). The pressure was again released immediately and the resulting suspension was treated with deionized water to neutral pH. In the decolorization step, the steam exploded chitin suspension were bleached using sodium chlorite ($NaClO_2$). After bleaching the suspension was thoroughly washed with distilled water. Finally, the filtered wet chitin was dispersed into water and sonicated in order to facilitate the formation of nano whiskers (Scheme 1).

2.3. Extraction of anthocyanin from butterfly pea flower

Extraction was done according to the method suggested by Pourjavaher (Pourjavaher et al., 2017).100g of Clitoria ternatea (CT) flower was blended and macerated with 1L of ethanol water mixture in the ratio (7:3). The sample was then stored in a refrigerator for 24 h.The solution was then filtered and centrifuged and the remaining extract, CTE was stored at 4 °C until use. (Scheme 2)

The total concentration of anthocyanins has been calculated from the following equation by implementing the pH differential method.

$$Anthocyanin\ pigment(cyanidin-3-glu\cos ide\ equivalents, mg \Big/ L = \frac{AxMWxDFx1000}{\varepsilon xL}$$

where A = Absorbance ($A_{520nm} - A_{700nm}$); pH 1.0 – ($A_{520nm} - A_{700nm}$); pH 4.5; MW (molecular weight) = 449.2 g/mol for cyanidin-3-glucoside; DF = dilution factor; L = pathlength in cm; ε = molar extinction coefficient for cyanidin-3-glucoside in L mol^{-1} cm^{-1}, and 1000 = factor for conversion from g to mg.

2.4. Preparation of films soy protein isolate composite films

The SPI and SPI composite films were prepared as follows. 5% (w/v) of SPI was magnetically stirred in water and 1.2 mL (40% w/v) glycerol

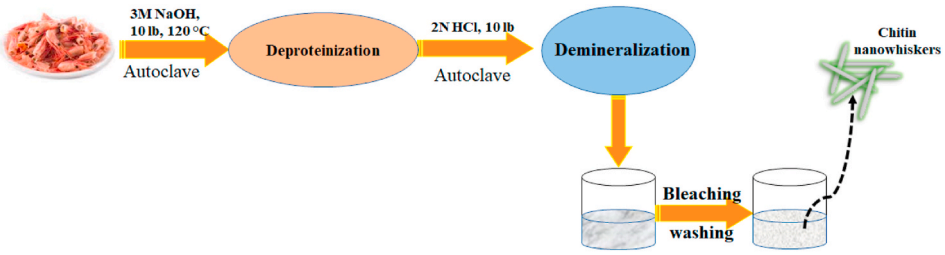

Scheme 1. Process of extraction of chitin nano whiskers from prawn shell waste.

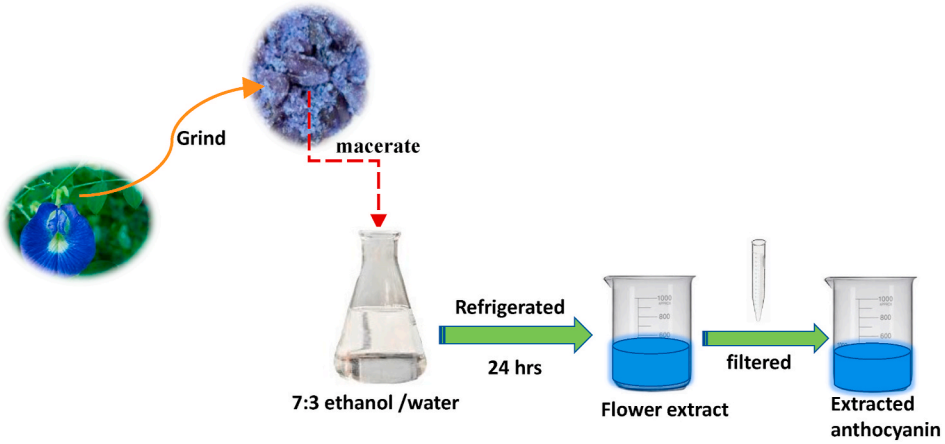

Scheme 2. Extraction process of anthocyanin from butterfly pea flowers.

was added as the plasticizer. The extract (CTE), and chitin nanowhisker (CNW) was added separately and homogenized (Ika Ultra-Turrax) by selecting the concentration as 8% (w/v). The selection of the weight percentage was after examining the colour given by these components to the composite films. pH was adjusted to 10. After that, the solution was magnetically stirred for 30min at 70 °C. Finally, film forming solution was cast onto Teflon plate and dried in an air oven at 55 °C. The samples were given the codes SPI, SPI-CNW, SPI-CTE and SPI-CNW-CTE.

2.5. Characterization

2.5.1. Transmission electron microscopy (TEM)

Transmission electron micrographs of CNW was obtained using a TEM, HT-7700, Hitachi Instruments Ltd at an accelerating voltage of 80 kV. A droplet of CNW dispersion was mounted on a carbon-coated copper grid and then washed dry.

2.5.2. X-ray diffraction analysis (XRD)

The XRD patterns of the raw chitin, CNW and SPI composites were measured with an XRD (Rigalku Miniflex 600 X-ray diffractometer) using Cu Kα radiation (λ = 1.5406 Å) as a source of X Ray and diffraction pattern recorded in the range 5°–40° at a scanning rate of 4°/min.

The Crystallinity Index (CI%) of CNW was calculated using the Segal empirical equation (Shankar et al., 2015):

$$CI = \frac{I(19) - I(12.6)}{I(19)} X\ 100\% \quad (1)$$

where I (19) represents the peak diffraction intensity corresponding to crystalline chitin and I (12.6) is the peak diffraction intensity of the amorphous chitin, at 2θ, values at 19 and 12.6, respectively.

The crystallite size (D) of the whisker was calculated by using the Scherrer equation (Shankar et al., 2015):

$$D = \frac{0.9\lambda}{\beta cos\theta} \quad (2)$$

where D is the crystal size, λ the wavelength of X-ray (0.15405 nm) θ the Bragg's angle.

2.5.3. Fourier transform infrared spectroscopy (FTIR)

FTIR microscopy of CNW and SPI composite films were done on a PerkinElmer Spectrum. FTIR spectrometer with Universal ATR accessory within the scan range of 4000–650 cm^{-1} with a total of 50 scans.

2.5.3.1. Degree of N-acetylation (DA) in chitin nano whisker using FTIR spectroscopy. DA can be determined by IR techniques in the following way:

$$DA\ (\%) = A_M/A_R x100$$

where AM(A_{1655}) is the intensity of the characteristic band of N-acetylation, and AR (A_{3450}) is the intensity of a reference band. The CNW formed is highly stable if DA value is greater than 50%. If the value is less than 50%, it confirms that the conversion of chitin to chitosan has taken place.

2.5.4. UV–visible spectrophotometer

UV–Visible absorbance of CNW was done using PerkinElmer Ltd., USA in the scan range between 190 and 500 nm.

2.5.5. Thermogravimetric analysis (TGA)

Thermo-gravimetric analysis of the CNW and composite films were performed using the Shimadzu TGA-Q500 instrument. Approximately 4–6 mg of the sample was heated at 10 °C/min under nitrogen atmosphere (50 mL/min) at 20–900 °C intervals.

2.5.6. Colour responses of anthocyanins in CTE to pH changes

CTE (1 mL) was dissolved in 30 mL of buffers with different pH values (pH 1.0–12.0) and the photographs of the solutions were taken.

2.5.7. Colour parameters of SPI, SPI-CNW, SPI-CTE and SPI-CNW-CTE films

Three colour parameters (L, a, b) of the films were determined using SC-80C colorimeter and the total colour difference was calculated using the formula

$$\Delta E = \sqrt{(L_0^* - L^*)^2 + (a_0^* - a^*)^2 + (b_0^* - b^*)^2}$$

where L_0^*, a_0^* and b_0^* were the color parameters of standard SPI film, and L^*, a^* and b^* were the colour parameters of composite films (Choi et al., 2017), (Wu et al., 2019).

2.5.8. Scanning electron microscopy (SEM)

SEM of composite films surfaces were done using Carl Zeiss Secondary Electron Microscope at an accelerating voltage of 20 kV.

2.5.9. Film thickness

A micrometre was used to measure the film thickness (Mitotuyo, no. 7327, Kawasaki, Japan). The thickness of each film form was determined in 4 random positions and average was calculated.

2.5.10. Moisture content

The moisture content of composite films was measured using a digital moisture analyser of MA 50. X2.A series. Triplicate measurement was done.

2.6. Statistical analysis

The Duncan test and one-way analysis of variance (ANOVA) were used for multiple comparisons by SPSS 13.0 software package. Difference was considered as statistically significant if $p < 0.05$.

3. Results and discussion

3.1. Characterisation of CNW

3.1.1. Transmission electron microscopy (TEM)

The TEM images of CNW is shown in Fig. 1(A). The nanowhisker suspensions consisted of single and aggregated nanocrystals in a blended state with individual CNW having a long,needle-like morphology with a broad range distribution in length from 100 to 400 nm and lateral diameters within 10–50 nm.

3.1.2. X-ray diffraction analysis (XRD)

Fig. 1(B) shows the X-ray diffraction patterns of raw chitin (CH) and CNW. Consistent with the reported values for CNW (Lu et al., 2013), the CNWs diffractogram showed sharp and well-defined peaks at (2θ) values of 9.57°, 19.7°, and 23.4° (corresponding to 020, 110 and 130 planes), showing highly crystalline structure. The diffraction peak at 29.6° showing the presence of calcium carbonate is completely absent indicating that complete removal of minerals during the demineralization process. The three diffraction peaks of CNWs observed at 9.57,19.7, and 23.4° corresponds to typical crystal patterns of α-chitin. Scherrer equation was used to calculate the crystal size and it was found to be in the range 5–10 nm. The prepared CNW was highly crystalline, with crystallinity index 99.67% (Equation (2)). This value was higher than the reported values (Huang et al., 2015; Fan et al., 2008) and this shows that pressure treatment is very effective in disaggregating chitin bundles into individual microfibrils and finally into nanostructures.

3.1.3. Fourier transform infrared spectroscopy (FTIR)

Fig. 1(C) shows the normalized FTIR spectra of the prepared CNW.

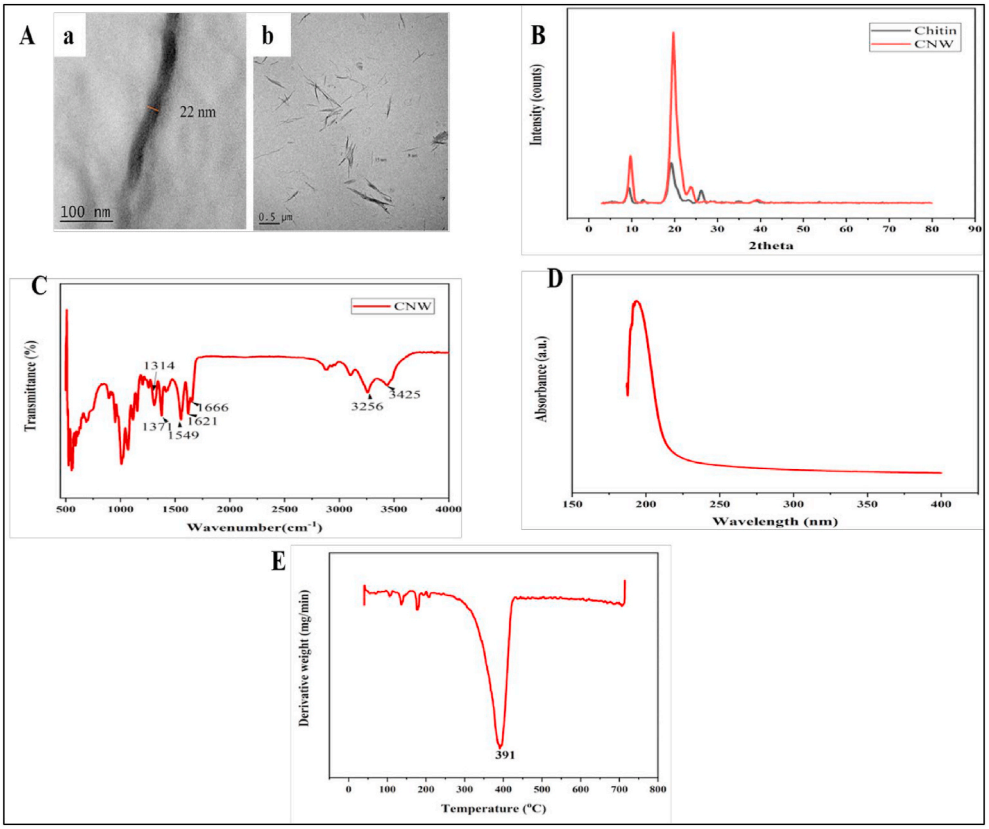

Fig. 1. (A) TEM images, (B) XRD patterns, (C) FTIR Spectra, (D) UV spectra and (E) DTG graph of chitin nanowhisker.

The FTIR spectrum showed the O–H and N–H stretching band at 3438 and 3257 cm^{-1}. The vibrational modes in the range 1660–1620 cm^{-1} corresponding to Amide I band can be used to distinguish α-and βchitin. The presence of two peaks in this range shows the formation of α-chitin structure (Sahraee et al., 2017). The peak in the range 1567–1553 cm^{-1} is attributed to amide II band corresponding to N–H bending and C–N stretch deformation in the CONH plane). The absence of peak at 1540 cm^{-1} confirmed that complete protein removal has taken place (Shankar et al., 2015). Peak observed at 1314 and 1372 cm^{-1} was attributed to C–H stretch of methyl groups. Amide III band corresponding to acetyl group was observed at 1260 cm^{-1}. The peak at 1156 cm^{-1} was assigned to stretching vibration of bridge oxygen (C(1)-O-C(4)) of glycosidic linkage (Lu et al., 2013). C–OH stretching vibration was observed at 1073 cm^{-1}. The peaks in the range 1018–1070 cm^{-1} were assigned to the saccharide structure present in carbohydrate backbone. The peak at 898 cm^{-1} showed C–H out of plane bending in glucose ring. The degree of acetylation (DA) value was found to be 91.17% which proves that the CNW formed is highly stable.

3.1.4. UV–visible spectrophotometer

The UV–Visible spectrum of CNW was found to exhibit a maximum absorption peak at ~195 nm (Fig. 1(D). This peak corresponds to the presence of chromophore groups N-acetyl glucosamine (GlcNc) and glucosamine (GlcN) present in chitin (Liu et al., 2006). The absorption band at 280 nm, due to aromatic amino acids (Ianiro et al., 2014) was completely absent in the spectra showing that successful deproteinization has taken place after alkaline treatment.

3.1.5. Thermogravimetric analysis (TGA)

The DTG curve of CNW is shown in Fig. 1(E). As evident from the figure, the first stage of weight loss due to loss of water occurred at 60°-100 °C. The second stage of weight loss for CNW occurred around 300 C - 450 °C. This weight loss was attributed to the degradation of the saccharide rings of the molecule, and the decomposition and polymerization of the and deacetylated and acetylated units of chitin. About 85% of the weight loss of CNW occurred in this stage. The DTG curve clearly shows that the maximum thermal decomposition of CNW occurred at 391 °C.The TGA curve of raw chitin at 313.3 °C shifted to 390.1 °C in nano chitin which suggests its high stability (Dhananasekaran et al., 2016) The third decomposition step corresponds to the remaining char and nonvolatile compounds CNW prepared in this study is found to have similar thermal stability than reported raw chitin (Shankar et al., 2015) and also higher than already reported CNW (Qin et al., 2016). The property was due to high crystalline index and DA and of CNW. The steam explosion pressure treatment exposed the polar moieties of CNW, (which was otherwise integrated within the proteinaceous matrix combined with calcium carbonate) resulting in the formation of stiffer and stronger network CNW structures, increasing the thermal stability. Similar result was obtained by Deepa et al. (2011) for the preparation of cellulose nano fibres from banana fibres by steam explosion.

Fig. 2. (A) Colour variations of CTE solution, (B) physical appearance of a) SPI, b) SPI-CNW, c) SPI-CTE and d) SPI-CNW-CTE films. (For interpretation of the references to colour in this figure legend, the reader is referred to the Web version of this article.)

3.2. Characterisation of SPI, SPI-CNW, SPI-CTE and SPI-CNW-CTE films

3.2.1. Anthocyanin concentration and colour of CTE in pH buffers

The anthocyanin content of 20.66 mg cyanidin-3-glucoside equivalent/L extract and an extraction yield of 16.6% based on dry weight of flower was obtained in this study. Fig. 2 (A) shows the colour variations of CTE in different pH buffers (1–12). As evident from the figure, the anthocyanin present in the extract solution exhibited wide colour variations ranging from red in pH (1–3), purple in pH (4–5), blue in pH (6–7), green in pH(8–9), colourless in pH(10–11) and yellow in pH (11–12). This colour changes is due to structural changes undergone by anthocyanin in different pH medium where it exhibit a red flavylium cationic structure at pH (1–3),a purple/blue quinoidal anhydro base at pH (4–7), green chalcone at pH (8–9), carbinol base at pH (10–11) and yellow chalcone at pH (12) (He et al., 2015).

3.2.2. Physical appearance of SPI composite films

Fig. 2(B) shows the physical appearance of SPI, SPI-CNW, SPI-CTE and SPI-CNW-CTE films. Table 1 shows the colour parameters values for the same. The colour of the films changed from yellow to green on addition of CTE extract. The L* values decreased on addition of CTE indicating that the film has become green in colour. On the other hand, ΔE value increased ($p < 0.05$) considerably on addition of CTE indicating that the film has become darker in colour and the colour change is visible by naked eye. Similar increase in ΔE was observed when mulberry polyphenolic extract was incorporated into κ-carrageenan film (Liu et al., 2019). The increased darker tone of SPI-CNW-CTE film will protect the food sample from UV oxidation and degradation preventing it from discolouration and nutrient loss.

3.2.3. Fourier transforms infrared (FT-IR) spectroscopy

FTIR spectroscopy (Fig. 3 (A)) details revealed that control and composite SPI films exhibited similar spectra with slight changes occurring in intensity or position of peaks. The control SPI film showed characteristic bands at 1631,1541 and1235cm^{-1}which can be assigned to amide I amide II and amide III band respectively. Amide I correspond to C–O stretching, amide II to N–H bending and amide III to C–H and N–H stretching. An increase in intensity of amide I band was observed on adding both CTE and CNW. This is because of the fact that C═O groups in CTE and CNW coincide with amide I band and its intensity gets enhanced. According to Choi et al. (2017), if there are noticeable band shifts in the FTIR spectra with the addition of fillers, it shows that a chemical interaction is present between the components. The shift in the amide III peak in SPI-CNW, SPI-CTE and SPI-CNW-CTE to lower values shows the possible hydrogen bonding interaction between SPI and the added fillers. The shift in wavenumber occurs when the N–H moiety in the peptide chain participate in hydrogen bonding. In this particular case the carboxyl and phenolic hydroxyl group of CTE extract and the hydroxyl group of CNW may form hydrogen bond with N–H group of protein. Similar shift was observed by Zhang et al. (2019a) when rosemary acid was added to rabbit skin gelatine films. The broad band at 3269 cm^{-1}is assigned to OH and NH stretching bands which can form hydrogen bonding with the carbonyl groups of protein molecule. On adding CNW and CTE this broad band becomes sharper and an increase in the wavenumber is observed indicative of the formation of hydrogen bond and electrostatic interactions in the composite film. However, no new peaks were observed on adding both CTE and CNW in SPI matrix revealing that no new covalent bonds were formed between SPI and CTE/CNW. Wu et al. (2019) also reported that only electrostatic and hydrogen bonding interactions occurred without any covalent bond formation when chitosan/oxidized chitin nanocrystals and black rice bran anthocyanins were added into chitosan matrix. All these evidences suggest that CTE anthocyanin was successfully immobilized in SPI matrix.

Table 1
Colour parameters including L*, a*, b*, ΔE of A) SPI, B) SPI-CNW, C) SPI-CTE and D) SPI-CNW-CTE films.

Films	L*	a*	b*	ΔE
SPI	73 ± 1.0^{a}	3 ± 1.04^{c}	31.3 ± 0.61^{b}	–
SPI + CNW	73.5 ± 0.5^{a}	3.5 ± 0.5^{c}	30.53 ± 0.81^{b}	1.31 ± 0.46^{b}
SPI + CTE	42.67 ± 0.58^{b}	−2 ±0.29^{b}	26.13 ± 0.32^{c}	31.65 ± 0.17^{a}
SPI + CNW + CTE	42 ± 1.0^{b}	1 ± 0.35^{a}	37.87 ± 0.81^{a}	32.23 ± 0.73^{a}

Standard deviation (±) is given. Different small case letters within the same column indicate significant differences ($p < 0.05$).

3.2.4. X-ray diffraction (XRD)

XRD patterns of SPI, SPI-CTE, SPI-CNW and SPI-CNW-CTE are shown in Fig. 3 (B). The pure SPI film shows characteristic peak at 2θ values of around 22^0 and 10.2^0 indicating amorphous nature of the matrix. The incorporation of CNW is found to increase the crystallinity of the SPI-CNW and SPI-CNW-CTE films. This can be attributed to higher crystallinity of CNW prepared using steam explosion technique and molecular interactions (hydrogen bonding and electrostatic) happening between SPI and CNW. The peak at 19.2^0 characteristic of CNW becomes prominent in XRD of SPI-CNW and SPI-CNW-CTE showing the incorporation of CNW in the matrix. Similar result was observed when oxidized chitin nanocrystal was added to chitosan matrix by Wu et al. (2019). The XRD spectra of SPI-CTE was found to be similar to control SPI which shows that the addition of CTE did not affect the crystallinity of SPI. These results were in accordance with the FTIR result. The incorporation of CTE can also lead to dilution effect on the matrix leading to the decrease in crystallinity compared to SPI-CNW films.

3.2.5. Thermal stability

Thermogram is used to understand the thermal stability of the material. Fig. 3(C) shows the thermogravimetric analysis of SPI, SPI-CTE, SPI-CNW and SPI-CNW-CTE. Similar to other films containing anthocyanin weight loss occurred in three stages in this case also. The first stage (70–100 °C) is assigned to the loss of water molecules. The second stage between 100 and 250 °C is assigned to loss of plasticizer, glycerol. The third stage occurs between 250 and 400 °C and is assigned to the decomposition of protein backbone and other fillers. From the thermogram it is quite clear that the addition of CNW has increased the thermal stability of the composite film. Both SPI-CNW and SPI-CNW-CTE films showed higher degradation temperature and heat resistance than control films. The thermogram of SPI and SPI-CTE were almost similar proving that no significant weight loss occurred on adding CTE to SPI matrix indicating that the addition of CTE did not affect the thermal stability of the film. Liang et al. also observed that addition of red cabbage anthocyanins into carboxymethyl cellulose film did not reinforce the thermal stability of the film (Liang et al., 2019).

3.2.6. Scanning electron microscopy (SEM)

The surface morphology of the films was analysed using SEM. The pure SPI had compact and smooth morphology due to homogenous dispersion of glycerol in the matrix (Fig. 3 (D)(a). With the addition CTE (Fig. 3 (D)(b)) the surface became smoother due to plasticizing effect of CTE changing the hydrogen bonds between the protein molecules. The addition of CNW in SPI matrix (Fig. 3(D)(c)) did not alter the surface of the film significantly as there was no pore formation or split structures indicating that CNW has been uniformly distributed in SPI matrix. However, the surface was not that compact as the one without CNW. Thus, the surface morphology of SPI films was not affected with the addition of fillers like CTE and CNW. This shows that the fillers were uniformly dispersed in SPI matrix. Oun et al. (Oun and Rhim, 2019) also observed that the surface morphology of carboxymethyl cellulose-based films incorporated with chitin nanocrystal and grapefruit seed extract did not change much with the addition of fillers.

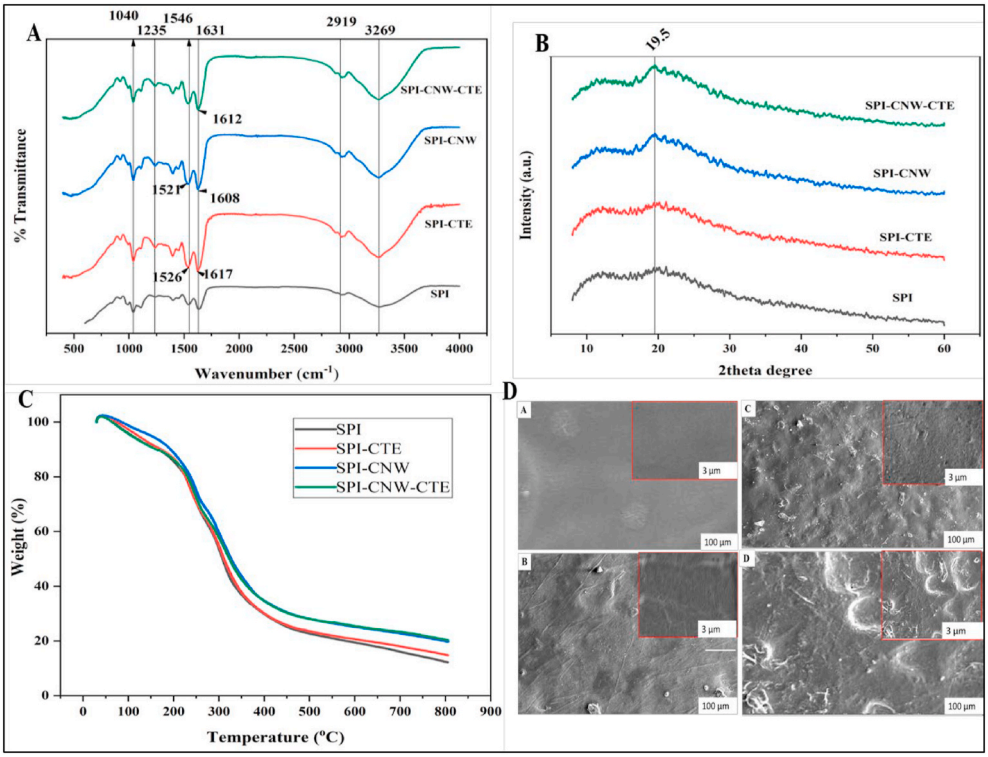

Fig. 3. (A) FTIR spectra, (B) XRD pattern, (C) TG curve of the films and (D) SEM analysis of a) SPI, (b) SPI-CTE, (c) SPI-CNW and d) SPI-CNW-CTE.

Table 2
Physical properties of the film.

Sample	Thickness (mm)	Moisture content (%)	Tensile strength (MPa)	Elongation at break (%)
SPI	0.23 ± 0.01	14.52	4.67 ± 0.79^{c}	59.02 ± 1.12^{b}
SPI-CTE	0.21 ± 0.04	14.36	3.61 ± 0.92^{d}	90.1 ± 5.52^{a}
SPI-CNW	0.20 ± 0.03	14.46	15.45 ± 0.95^{a}	7.05 ± 1.75^{d}
SPI-CNW-CTE	0.19 ± 0.03	13.82	13.25 ± 0.47^{b}	38.46 ± 3.2^{c}

Standard deviation (±) is given. Different small case letters within the same column indicate significant differences ($p < 0.05$).

3.2.7. Film thickness and moisture content

Thickness value of SPI and SPI composite films are shown in Table 2. No marked difference in thickness was observed between SPI film and SPI composite films. This indicated that both CNW and CTE are homogenously dispersed in the matrix. Due to abundant OH groups in both CTE and CNW both this additive can closely combine like a bridge with protein matrix through intermolecular interactions. Similar result was observed by Wang et al. (2019) when black soybean seed coat was incorporated in chitosan matrix. As presented in Table 2 no significant difference in moisture content was observed between SPI and SPI composite films. This is attributed to the fact that SPI is itself hydrophilic and the addition of hydrophilic anthocyanin and CNW results in more polar groups which can absorb moisture from the surroundings. But due to network structure between SPI/CNW/CTE the composite films exhibit slightly less moisture content than control. Yong et al. (2019) also observed that there was no decrease in moisture content of chitosan film when purple and black eggplant was incorporated in its matrix.

3.2.8. Mechanical properties

Tensile strength of SPI and elongation at break values of SPI and SPI composite films are summarised in Table 2. The tensile strength values increased from 4.67 MPa to 15.45 MPa for SPI-CNW film. The increase in mechanical property shows that the incorporation of CNW in SPI matrix results in strong interactions between SPI and CNW limiting the matrix motion. The CNW is found to enhance the mechanical properties of nanocomposite films owing to the creation of strong network through enhanced hydrogen bonds, higher stiffness and density in CNW compared to protein matrix, filling of hollow spaces in amorphous regions and increasing the crystallinity of the matrix. However, the tensile strength slightly decreased with the incorporation of CTE in SPI-CNW matrix owing to plasticization effect of CTE disrupting the bond between SPI and CNW which thereby promote mobility of the polymer chain and breaking the compact rigid structure between SPI and CNW. Comparable result was obtained when oxidized chitin nanocrystals and black rice bran anthocyanins was incorporated in chitosan matrix (Wu et al., 2019), roselle anthocyanins was incorporated in starch-polyvinyl alcohol films (Zhai et al., 2017), red cabbage anthocyanins was added to artemisia sphaerocephala krasch. gum/carboxymethyl cellulose film (Liang et al., 2019). The elongation at break value is an indication of the flexibility of the films. As evident from the Table 2 elongation at break value was highest for SPI-CTE film. This may be attributed to the repulsive forces acting between phenols and flavonoids in the extract leading to the weaking of forces between the protein chains. Tan et al., also have reported that elongation at break value of chitosan film increased with increased concentration of grapefruit seed extract in the matrix. The elongation at break value decreased with the addition of CNW owing to the crosslinking between the matrix and CNW leading to a more compact structure (Tan et al., 2015).

3.2.9. pH-sensitive ability of SPI, SPI-CNW, SPI-CTE and SPI-CNW-CTE films

The SPI films containing anthocyanin extract is found to exhibit different colours in different pH media. This is attributed to the structural changes of anthocyanin in different pH. Anthocyanin is found to exist as flavylium cation which is red in colour at (pH < 4), as carbinol base which is colourless at (pH~ 4–5), as quinoidal anhydro base which is purple/blue in colour at (pH ~6–8) and as chalcone which is light yellow at (pH > 8). As evident from Fig. 4(A)(a & b) the control SPI film

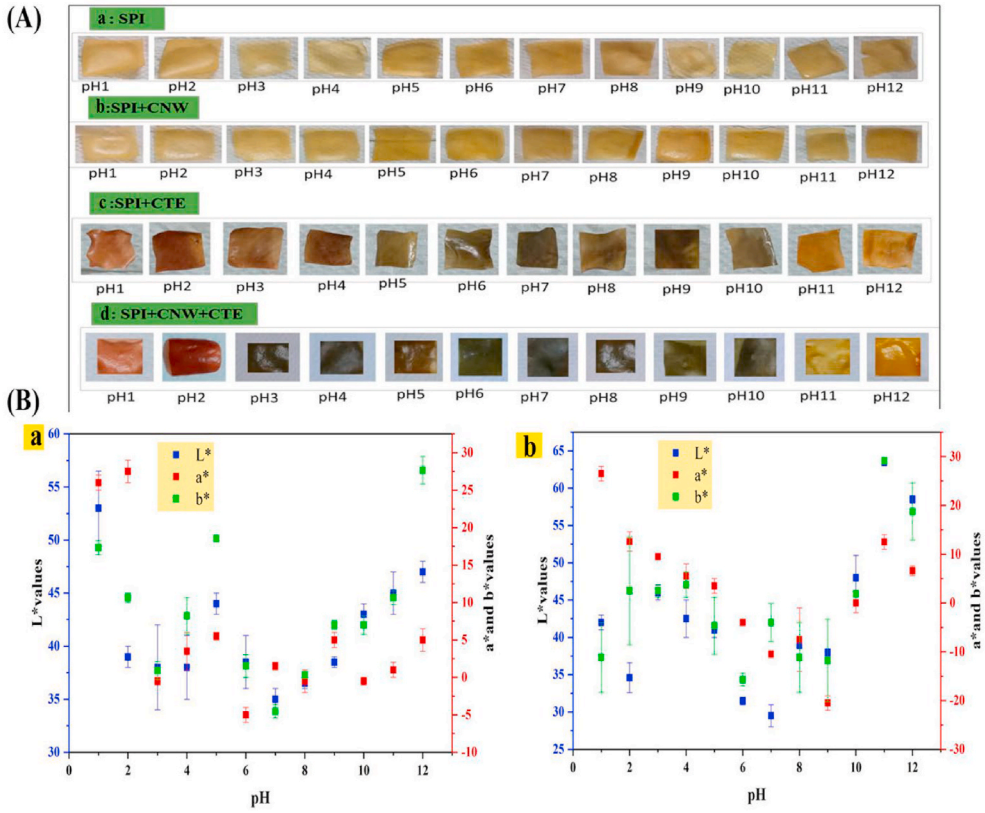

Fig. 4. (A) The visible colours of SPI and SPI films with CTE and CNW in different pH range (1–12), (B) Colour parameters L*, a*, b*of (a) SPI-CTE film and (b) SPI-CNW-CTE film. Standard deviations of triplicate measurement are given as vertical bars. (For interpretation of the references to colour in this figure legend, the reader is referred to the Web version of this article.)

Table 3
The ΔE values of SPI, SPI-CNW, SPI-CTE and SPI-CNW-CTE films after being exposed to different buffer solutions for 5 min.

pH	SPI Film	SPI + CNW Film	SPI + CTE Film	SPI + CNW + CTE
1	2.71 ± 1.42^{gD}	9.95 ± 1.52^{aC}	40.21 ± 0.44^{bB}	45.40 ± 2.06^{aA}
2	5.08 ± 0.54^{efC}	2.81 ± 1.06^{defD}	37.85 ± 2.22^{cB}	46.20 ± 0.92^{aA}
3	7.73 ± 0.73^{cdD}	11.44 ± 1.39^{aC}	26.40 ± 1.31^{fB}	34.26 ± 0.48^{efA}
4	9.77 ± 0.07^{bC}	1.67 ± 0.50^{fD}	29.52 ± 1.22^{eB}	38.37 ± 0.62^{bA}
5	5.17 ± 1.13^{fD}	6.5 ± 0.21^{bC}	32.19 ± 0.39^{dB}	45.74 ± 0.12^{aA}
6	2.36 ± 0.8^{gD}	5.14 ± 1.32^{bcC}	44.53 ± 1.34^{aA}	35.80 ± 0.63^{deB}
7	7.08 ± 0.77^{cdC}	4.31 ± 0.63^{cdeD}	45.04 ± 1.02^{aA}	35.90 ± 0.53^{cdB}
8	6.77 ± 0.62^{deC}	2.64 ± 0.81^{efD}	37.56 ± 1.22^{cA}	35.48 ± 0.51^{deB}
9	8.76 ± 1.13^{bcC}	4.51 ± 1.24^{cdD}	44 ± 0.29^{aA}	37.11 ± 0.80^{bcB}
10	9.88 ± 0.87^{bC}	1.51 ± 0.22^{fD}	23.43 ± 1.38^{gB}	33.11 ± 0.42^{fA}
11	8.22 ± 0.7^{cdC}	2.37 ± 0.14^{fD}	19.01 ± 0.23^{hB}	35.49 ± 0.04^{deA}
12	11.73 ± 0.38^{aC}	2.36 ± 1.19^{fD}	14.74 ± 1.18^{iB}	27.55 ± 0.38^{gA}

Values are expressed as mean ± SD (n = 3). Different lower-case letters in the same column indicate significantly different ($p < 0.05$). Different capital letters in the same row indicate significantly different ($p < 0.05$).

and SPI-CNW did not show any colour changes in different pH due to the absence of anthocyanin in it. SPI-CTE and SPI-CNW-CTE film (Fig. 4(A) c & d) exhibited visual colour changes ranging from red in acidic pH through green in neutral pH to yellow in basic pH. Similar response to pH was observed in other anthocyanin enriched films such as chitosan/black plum peel extract film (Zhang et al., 2019b), chitosan/corn starch film/red cabbage film (Silva-Pereira et al., 2015) etc. Colour parameters (ΔE) of different films at pH 1–12 were compared and summarized in Table 3. Both SPI-CTE and SPI-CNW-CTE film presented high ΔE values compared to control SPI and SPI-CNW films at same pH conditions ($p < 0.05$). The ΔE values was also found to first increase and then decrease with increase in pH for films containing anthocyanin. Similar trend was observed by Huimin et al. (Yong et al., 2019) and Xingchi et al. (Wang et al., 2019) for chitosan film immobilized with purple/black eggplant and black soybean coat extract. Hence our films containing anthocyanin can function as pH sensitive indicators.

4. Conclusion

Highly crystalline CNWs were prepared under neutral condition employing the steam explosion procedure and the nanowhisker was used to fabricate SPI-CNW composite films by the incorporation of anthocyanin from Clitoria ternatea flower extract. The X-ray diffraction studies revealed that the nanowhiskers have size between 6.051 nm and 9.058 nm with a crystallinity index of 99.67%, that suggests highly crystalline structure. From the TEM images, it was found that the CNW possessed a needle like morphology. The synthesized CNW was used as reinforcing agent in soy protein matrix to fabricate SP-CNW nanocomposites. The addition of chitin nano whiskers enhanced the mechanical properties, especially the tensile strength with an addition of 8% (w/v) of CNW. Anthocyanin extracted from *Clitoria ternatea* was immobilized in this SPI-CNW matrix to make it pH sensitive. This pH indicator film is non toxic and produce reliable color changes in acidic and basic mediums. Hence it is suggested to be used to monitor the freshness of packed food products.

CRediT authorship contribution statement

Rekha Rose Koshy: Concept, execution, lab-work,writing(major). **Arunima Reghunadhan:** Writing(minor), correction, interpretation, illustration. **Siji K. Mary:** Concept, execution, lab-work. **Prasanth S. Pillai:** Formal analysis. **Seno Joseph:** Supervision. **Laly A. Pothen:** Supervision.

Declaration of competing interest

The authors declare that they have no known competing financial interests or personal relationships that could have appeared to influence the work reported in this paper.

Acknowledgement

The authors would like to thank Common Instrumentation Facility Centre (CLIF), Kerala University for doing the characterisation of the films.

References

Ahmad, N.A., Yook Heng, L., Salam, F., Mat Zaid, M.H., Abu Hanifah, S., 2019. A colorimetric pH sensor based on Clitoria sp and Brassica sp for monitoring of food spoilage using chromametry. Sensors 19. https://doi.org/10.3390/s19214813.

Choi, I., Lee, J.Y., Lacroix, M., Han, J., 2017. Intelligent pH indicator film composed of agar/potato starch and anthocyanin extracts from purple sweet potato. Food Chem 218, 122–128. https://doi.org/10.1016/j.foodchem.2016.09.050.

Deepa, B., Abraham, E., Cherian, B.M., Bismarck, A., Blaker, J.J., Pothan, L.A., Leao, A. L., de Souza, S.F., Kottaisamy, M., 2011. Structure, morphology and thermal characteristics of banana nano fibers obtained by steam explosion. Bioresour. Technol. 102, 1988–1997. https://doi.org/10.1016/j.biortech.2010.09.030.

Dhananasekaran, S., Palanivel, R., Pappu, S., 2016. Adsorption of methylene blue, bromophenol blue, and coomassie brilliant blue by α-chitin nanoparticles. J. Adv. Res. 7, 113–124. https://doi.org/10.1016/j.jare.2015.03.003.

Fan, Y., Saito, T., Isogai, A., 2008. Chitin nanocrystals prepared by TEMPO-mediated oxidation of α-chitin. Biomacromolecules 9, 192–198. https://doi.org/10.1021/bm700966g.

He, X., Li, X., Lv, Y., He, Q., 2015. Composition and Color Stability of Anthocyanin-Based Extract from Purple Sweet Potato, vol. 35, pp. 468–473.

Huang, Y., Yao, M., Zheng, X., Liang, X., Su, X., Zhang, Y., Lu, A., Zhang, L., 2015. Effects of chitin whiskers on physical properties and osteoblast culture of alginate based nanocomposite hydrogels. Biomacromolecules 16, 3499–3507. https://doi.org/10.1021/acs.biomac.5b00928.

Ianiro, A., Giosia, M.D., Fermani, S., Samorì, C., Barbalinardo, M., Valle, F., Pellegrini, G., Biscarini, F., Zerbetto, F., Calvaresi, M., Falini, G., 2014. Customizing properties of β-chitin in squid pen (gladius) by chemical treatments. Mar. Drugs . 12 https://doi.org/10.3390/md12125979.

Ifuku, S., Saimoto, H., 2012. Chitin nanofibers: preparations, modifications, and applications. Nanoscale 4, 3308–3318. https://doi.org/10.1039/c2nr30383c.

Ifuku, S., Morooka, S., Morimoto, M., Saimoto, H., 2010. Acetylation of chitin nanofibers and their transparent nanocomposite films. Biomacromolecules 11, 1326–1330. https://doi.org/10.1021/bm100109a.

Ifuku, S., Nogi, M., Abe, K., Yoshioka, M., Morimoto, M., Saimoto, H., Yano, H., 2011. Simple preparation method of chitin nanofibers with a uniform width of 1P_20nm from prawn shell under neutral conditions. Carbohydr. Polym. 84, 762–764.

Kaushik, A., Singh, M., Verma, G., 2010. Green nanocomposites based on thermoplastic starch and steam exploded cellulose nanofibrils from wheat straw. Carbohydr. Polym. 82, 337–345. https://doi.org/10.1016/j.carbpol.2010.04.063.

Liang, T., Sun, G., Cao, L., Li, J., Wang, L., 2019. A pH and NH3 sensing intelligent film based on Artemisia sphaerocephala Krasch. gum and red cabbage anthocyanins anchored by carboxymethyl cellulose sodium added as a host complex. Food Hydrocoll 87, 858–868. https://doi.org/10.1016/j.foodhyd.2018.08.028.

Liu, D., Wei, Y., Yao, P., Jiang, L., 2006. Determination of the degree of acetylation of chitosan by UV spectrophotometry using dual standards. Carbohydr. Res. 341, 782–785. https://doi.org/10.1016/j.carres.2006.01.008.

Liu, Y., Qin, Y., Bai, R., Zhang, X., Yuan, L., Liu, J., 2019. Preparation of pH-sensitive and antioxidant packaging films based on κ-carrageenan and mulberry polyphenolic extract Yunpeng. Int. J. Biol. Macromol. 134, 993–1001.

Lu, Y., Sun, Q., She, X., Xia, Y., Liu, Y., Li, J., Yang, D., 2013. Fabrication and characterisation of α-chitin nanofibers and highly transparent chitin films by pulsed ultrasonication. Carbohydr. Polym. 98, 1497–1504. https://doi.org/10.1016/j.carbpol.2013.07.038.

Luchese, C.L., Abdalla, V.F., Spada, J.C., Tessaro, I.C., 2018. Evaluation of blueberry residue incorporated cassava starch film as pH indicator in different simulants and foodstuffs. Food Hydrocoll 82, 209–218. https://doi.org/10.1016/j.foodhyd.2018.04.010.

Oun, A.A., Rhim, J.W., 2019. Preparation of multifunctional carboxymethyl cellulose-based films incorporated with chitin nanocrystal and grapefruit seed extract. Int. J. Biol. Macromol. https://doi.org/10.1016/j.ijbiomac.2019.10.191.

Pourjavaher, S., Almasi, H., Meshkini, S., Pirsa, S., Parandi, E., 2017. Development of a colorimetric pH indicator based on bacterial cellulose nanofibers and red cabbage (Brassica oleraceae) extract. Carbohydr. Polym. 156, 193–201. https://doi.org/10.1016/j.carbpol.2016.09.027.

Qin, Y., Zhang, S., Yu, J., Yang, J., Xiong, L., Sun, Q., 2016. Effects of chitin nano-whiskers on the antibacterial and physicochemical properties of maize starch films. Carbohydr. Polym. 147, 372–378. https://doi.org/10.1016/j.carbpol.2016.03.095.

Sahraee, S., Milani, J.M., Ghanbarzadeh, B., Hamishehkar, H., 2017. Physicochemical and antifungal properties of bio-nanocomposite film based on gelatin-chitin nanoparticles. Int. J. Biol. Macromol. 97, 373–381. https://doi.org/10.1016/j.ijbiomac.2016.12.066.

Shankar, S., Reddy, J.P., Rhim, J.-W., Kim, H.-Y., 2015. Preparation, characterization, and antimicrobial activity of chitin nanofibrils reinforced carrageenan nanocomposite films. Carbohydr. Polym. 117, 468–475. https://doi.org/10.1016/j.carbpol.2014.10.010.

Silva-Pereira, M.C., Teixeira, J.A., Pereira-Júnior, V.A., Stefani, R., 2015. Chitosan/corn starch blend films with extract from Brassica oleraceae (red cabbage) as a visual indicator of fish deterioration. LWT - Food Sci. Technol. 61, 258–262. https://doi.org/10.1016/j.lwt.2014.11.041.

Tan, Y.M., Lim, S.H., Tay, B.Y., Lee, M.W., Thian, E.S., 2015. Functional chitosan-based grapefruit seed extract composite films for applications in food packaging technology. Mater. Res. Bull. 69, 142–146. https://doi.org/10.1016/j.materresbull.2014.11.041.

Vijayalakshmi, K., Bm, D., Pn, S., Venkatesan, J., Anil, S., 2016. Nanomedicine & Nanotechnology Synthesis , Characterization and Applications of Nanochitosan/Sodium Alginate/Microcrystalline Cellulose Film, vol. 7. https://doi.org/10.4172/2157-7439.1000419.

Wang, X., Yong, H., Gao, L., Li, L., Jin, M., Liu, J., 2019. Preparation and characterization of antioxidant and pH-sensitive films based on chitosan and black soybean seed coat extract. Food Hydrocoll 89, 56–66. https://doi.org/10.1016/j.foodhyd.2018.10.019.

Wu, C., Sun, J., Zheng, P., Kang, X., Chen, M., Li, Y., Ge, Y., Hu, Y., Pang, J., 2019. Preparation of an intelligent film based on chitosan/oxidized chitin nanocrystals incorporating black rice bran anthocyanins for seafood spoilage monitoring. Carbohydr. Polym. 222, 115006 https://doi.org/10.1016/j.carbpol.2019.115006.

Yong, H., Wang, X., Zhang, X., Liu, Y., Qin, Y., Liu, J., 2019. Effects of anthocyanin-rich purple and black eggplant extracts on the physical, antioxidant and pH-sensitive properties of chitosan film. Food Hydrocoll 94, 93–104. https://doi.org/10.1016/j.foodhyd.2019.03.012.

Yun, D., Cai, H., Liu, Y., Xiao, L., Song, J., Liu, J., 2019. Development of active and intelligent films based on cassava starch and Chinese bayberry (Myrica rubra Sieb. et Zucc.) anthocyanins. RSC Adv 9, 30905–30916. https://doi.org/10.1039/C9RA06628D.

Zhai, X., Shi, J., Zou, X., Wang, S., Jiang, C., Zhang, J., Huang, X., Zhang, W., Holmes, M., 2017. Novel colorimetric films based on starch/polyvinyl alcohol incorporated with roselle anthocyanins for fish freshness monitoring. Food Hydrocoll 69, 308–317. https://doi.org/10.1016/j.foodhyd.2017.02.014.

Zhang, X., Ma, L., Yu, Y., Zhou, H., Guo, T., Dai, H., Zhang, Y., 2019a. Physico-mechanical and antioxidant properties of gelatin film from rabbit skin incorporated with rosemary acid. Food Packag. Shelf Life. 19, 121–130. https://doi.org/10.1016/j.fpsl.2018.12.006.

Zhang, X., Liu, Y., Yong, H., Qin, Y., Liu, J., Liu, J., 2019b. Development of multifunctional food packaging films based on chitosan, TiO2 nanoparticles and anthocyanin-rich black plum peel extract. Food Hydrocoll 94, 80–92. https://doi.org/10.1016/j.foodhyd.2019.03.009.

Zolfi, M., Khodaiyan, F., Mousavi, M., Hashemi, M., 2014. Development and characterization of the kefiran-whey protein isolate-TiO2 nanocomposite films. Int. J. Biol. Macromol. 65, 340–345. https://doi.org/10.1016/j.ijbiomac.2014.01.010.